Photodissociation of NeBr2(B) below and above the dissociation limit of Br2(B)

Octavio Roncero, José Campos-Martínez, Marta I. Hernández, Gerardo Delgado-Barrio, Pablo Villarreal et al.

Citation: J. Chem. Phys. **115**, 2566 (2001); doi: 10.1063/1.1386648
View online: http://dx.doi.org/10.1063/1.1386648
View Table of Contents: http://jcp.aip.org/resource/1/JCPSA6/v115/i6
Published by the American Institute of Physics.

Photodissociation of $NeBr_2(B)$ below and above the dissociation limit of $Br_2(B)$

Octavio Roncero, José Campos-Martínez, Marta I. Hernández, Gerardo Delgado-Barrio, and Pablo Villarreal
Instituto de Matemáticas y Física Fundamental, C.S.I.C., Serrano 123, 28006 Madrid, Spain

J. Rubayo-Soneira
Instituto Superior de Ciencias y Tecnología Nucleares, Habana 10600, Cuba

(Received 19 April 2001; accepted 29 May 2001)

The photodissociation dynamics of the $NeBr_2$ complex in the B electronic state is studied, for the first time, near the $Br_2(B)$ dissociation limit, below and above, when the complex is promoted from the ground T-shaped level in the X electronic state. A time-dependent treatment is used in which the initial wave packet is divided in two portions, one describing the slow predissociation dynamics below the Br_2 dissociation threshold, and the second one, the fast complete dissociation in Ne+Br+Br fragments. Below that threshold, the absorption spectrum shows an increasing congestion as the vibrational energy content of Br_2 increases, but narrow peaks appear again for the highest energy region of the spectrum. These peaks correspond to long lived resonances associated with ''horseshoe'' type states, as demonstrated by two-dimensional calculations. These resonances have a significant probability density for the linear geometry in which the Ne atom is inserted between the two bromine atoms. At this configuration the exchange of vibrational energy is rather inefficient which explains both why the spectrum is so sparse and resonances are so narrow. Above the Br_2 dissociation threshold, the recombination of Br_2 is found to be very inefficient, except for very low kinetic energies. The small recombination probabilities are due to vibrational couplings and not to any collisional caging effect. Since the complex remains essentially T-shaped during dissociation, extensive two-dimensional calculations are performed for longer times to better determine final vibrational distributions at low kinetic energies. [DOI: 10.1063/1.1386648]

I. INTRODUCTION

Rare gas-dihalogen van der Waals complexes, X–BC, provide nice examples of quite a wide variety of fundamental photophysical processes.[1–3] Despite their apparent simplicity that makes possible accurate theoretical calculations and modeling, they present abundant allowed spectroscopic transitions, specially from the ground to the B excited electronic state. Due to the natural separation between the ''fast'' intramolecular BC vibration and the ''slow'' van der Waals modes, it is possible to prepare these systems in a highly excited vibrational level of the BC subunit, v', and monitor its decay into the dissociative continua, in the same or in a different electronic state, i.e., through vibrational or electronic predissociation, respectively. Vibrational predissociation (VP) takes place by the transfer of one or several vibrational quanta from the BC subunit to the weaker van der Waals bond that eventually breaks up.

When only one vibrational quantum is required to fragment the system ($\Delta v=-1$ regime), the metastable levels reached through optical excitation usually decay following an exponential law. The associated lifetime decreases monotonically with vibrational excitation due to the decrease of the available kinetic energy in the $v'-1$ manifold, as stated by the energy[4] or momentum[5] gap laws. Such a behavior has been confirmed for several of these complexes, especially those involving He, like HeI_2 (Refs. 6,7) and $HeCl_2$,[8] or Ne atoms, like NeI_2,[9,10] $NeBr_2$,[11] and $NeCl_2$.[12]

As vibrational excitation becomes larger, the number of vibrational quanta, Δv, needed to fragment the system increases and intramolecular vibrational relaxation (IVR) among several quasibound zero-order levels of different vibrational manifolds of the BC molecule competes with VP. In this case the decay is no longer exponential and the spectra become rather complicated. Such a situation has been studied for $ArCl_2$,[13–16] ArI_2,[17–19] and $HeBr_2$.[20–24] The binding energy of the complex increases with the mass of the rare gas atom, and the number of states involved in the IVR becomes larger. A question arising at this point is whether or not so small systems can present IVR in the statistical limit, traditionally attributed to large systems. This issue has been addressed before, and extensive calculations have been performed for $ArCl_2$,[16] to analyze the effect of initial vibrational and rotational excitation of the complex. Unfortunately, there are not available experimental data for $v'>12$, because after this level ''dark'' electronic predissociation (EP) becomes dominant.[13]

The competition between EP and VP has been extensively studied in ArI_2,[25–33] and the modeling of the dynamics, involving nonadiabatic couplings among several electronic states, becomes so complicated that there is no present explanation for some experimental observations which are

apparently contradictory.[25,33] A complete theoretical description of the ArI_2 dynamics is rather difficult, since it involves obtaining several potential energy surfaces and their couplings, and accurate dynamical calculations afterwards. Nowadays there is an increasing number of diatom-in-molecules models[34,35] for the calculation of the excited electronic states involved in this kind of processes.

One goal of this work is the characterization of IVR in the high density of states regime on a single electronic state, to avoid the complications introduced by EP. To this purpose, the $NeBr_2$ complex is a good prototype. It has been experimentally studied over a wide range of vibrational excitations,[11,36–38] up to $v'=30$, and there has been no observed significant reduction in fluorescence with increasing linewidth.[11] It is therefore expected that nonadiabatic transitions do not play an important role for this system and that only the B electronic state is needed to describe the dynamics. There are several theoretical studies[39–41] on the VP dynamics, for which dissociation takes place by the transfer of a single vibrational quantum up to $v'=27$, where the $\Delta v=-1$ closes, in accordance with experiment. For $v'>30$, where IVR effects are expected, there are no studies neither experimental nor theoretical.

In this work we study the fragmentation dynamics of $NeBr_2$ near the dissociation threshold of $Br_2(B)$. Below this threshold, the dominant process is

$$\begin{aligned}&\mathrm{Ne}\cdots\mathrm{Br}_2(X,v=0)+\hbar\omega\\&\quad\rightarrow[\mathrm{Ne}\cdots\mathrm{Br}_2(B,v')]^*\\&\quad\rightarrow\mathrm{Br}_2(B,v''=v'-\Delta v,j'')+\mathrm{Ne},\end{aligned}\tag{1}$$

where it is interesting to analyze the effect of the density of quasibound levels on the VP mediated by IVR and, in particular, near the Br_2 dissociation limit where the spectrum may congest and the IVR regime could reach the statistical limit. Above the dissociation threshold, the main process is the complete fragmentation of the system,

$$\mathrm{Ne}\cdots\mathrm{Br}_2(X,v=0)+\hbar\omega\rightarrow\mathrm{Ne}+\mathrm{Br}+\mathrm{Br},\tag{2}$$

where it would be of great interest to find out to what extent the recombination process, i.e., the formation of $Br_2(B,v'')$, is possible. Results on the recombination of Br_2 will be discussed in comparison with the related system ArI_2, which has been extensively studied both experimentally and theoretically.[33,42–51]

The study of such processes is performed in grids using time-dependent wave packet methods, as briefly described in Sec. II. The dynamics below and above the $Br_2(B)$ threshold is reported and discussed in Secs. III and IV, respectively. Finally, Sec. V is devoted to some conclusions.

II. QUANTUM TIME-DEPENDENT DYNAMICS

The methodology used for the quantum study has been described elsewhere[52] and will only be presented briefly here. In the present treatment, **r** and **R** Jacobi coordinates are used, where **r** is the Br_2 internuclear vector, and **R** is the vector joining the Br_2 center of mass to the Ne atom (with $\mathbf{R}\cdot\mathbf{r}=rR\cos\gamma$). These vectors are expressed in a body-fixed frame such that the z-axis lies along **R** and the three atoms are in the $x-z$ plane. The orientation of the body-fixed axes with respect to the space-fixed frame is specified by three Eulerian angles[53] (θ,ϕ,χ). In this representation the total wave packet is expanded as[16,54]

$$\Psi^{JM\epsilon}(\mathbf{R},\mathbf{r},t)=\sum_{\Omega}\ W^{J\epsilon}_{M\Omega}(\phi,\theta,\chi)\frac{\Phi^{JM\epsilon}_{\Omega}(r,R,\gamma,t)}{rR},\tag{3}$$

where the functions $W^{J\epsilon}_{M\Omega}$ are linear combinations of Wigner rotation matrices,[53] corresponding to a total angular momentum J, such that ϵ is the parity under inversion of spatial coordinates. M and Ω are the projections of the total angular momentum on the space-fixed and body-fixed z-axis, respectively.

The integration of the time-dependent Schrödinger equation is accomplished, as described previously,[16,54] using the Chebyshev method[55] and the $\Phi^{JM\epsilon}_{\Omega}(r,R,\gamma,t)$ coefficients are represented on finite grids for the internal coordinates r, R, and γ. A set of equidistant points is chosen for each radial grid, and the radial kinetic terms are obtained using the fast Fourier transform method.[56] In order to avoid spurious reflections, the wave packet is absorbed at each time step.[57–59] For γ we use a DVR representation[16,60–64] formed by a set of Gauss–Legendre quadrature points.

In this work we study electric dipole transitions from an initial bound state $\Psi^{J_iM_i\epsilon_i}_{i}$, with energy E_i in the X ground electronic state and total angular momentum J_i, to final dissociative states in the excited B electronic state and total angular momentum J. Defining the $\Phi^{JM\epsilon}_{\Omega}(r,R,\gamma,t)$ components of the initial wave packet as[52]

$$\Phi^{JM\epsilon}_{\Omega}(r,R,\gamma,t=0)=\langle W^{J\epsilon}_{M\Omega}|\mathbf{d}\cdot\mathbf{e}|\Psi^{J_iM_i\epsilon_i}_{i}\rangle,\tag{4}$$

the total absorption cross section, within the framework of first order perturbation theory, is given by[65,66]

$$\sigma(E)\propto\frac{1}{2\pi\hbar}\int_{-\infty}^{\infty}dt e^{iEt/\hbar}\langle\Psi^{JM\epsilon}(\mathbf{R},\mathbf{r},t=0)|\Psi^{JM\epsilon}(\mathbf{R},\mathbf{r},t),\rangle,\tag{5}$$

where **e** is the polarization vector of the incident photon and **d** is the electric dipole transition moment. The latter is assumed to be located along the **r** vector, because Br_2 is the responsible of the oscillator strength for the parallel $B\leftarrow X$ transition, and its components, in the body-fixed frame, are

$$d_q(r,R,\gamma)\propto D^{1*}_{q0}(0,\gamma,0).\tag{6}$$

Partial cross sections corresponding to final rovibrational states of the $Br_2(v'',j'')$ fragments are obtained using the method of Balint-Kurti *et al.*[67]

The simultaneous simulation of fast and slow processes involves a great difficulty. In the present case, the dynamics is rather slow below the dissociation threshold, which requires long propagation times, while above that limit the dynamics is fast and the spectrum very broad, which requires much shorter time steps and denser grids. In order to reduce the computational cost, the initial wave packet is divided in several portions using the projection operators

$$P=\sum_v P_v; \quad Q=1-P, \tag{7}$$

with

$$P_v=\sum_j \sum_\Omega |F_{vj\Omega}\rangle\langle F_{vj\Omega}|, \tag{8}$$

and

$$F_{vj\Omega}=\frac{\varphi_{vj}(r)}{r} Y_{j\Omega}(\gamma,0) W^{J\epsilon}_{M\Omega}(\phi,\theta,\chi). \tag{9}$$

Dealing with a linear differential equation, the propagation of the different portions of the initial wave packet is essentially exact. Total or partial cross sections would be then obtained by reconstructing the total wave packet at each time. This procedure, however, presents the problem of storing the different portions of the wave packet. A possible approximation is to evaluate cross sections for each portion of the wave packet separately, thus neglecting interference terms. When the different portions of the spectrum present a negligible overlap, this approach becomes quite accurate, as in the case of isolated resonances.

In this work, the $J=0\leftarrow J_i=1$ transition is studied and the total wave packet is divided in two portions, Ψ_P and Ψ_Q, corresponding to energies below and above the $Br_2(B)$ threshold, respectively. The initial Ψ_P and Ψ_Q portions correspond to those parts of the total initial wave packet which overlaps with the bound vibrational and continuum dissociative states, respectively, of $Br_2(B)$. These two parts would be uncoupled in the case of bare Br_2, but, since the propagation is numerically " exact," the dynamics of Ψ_P and Ψ_Q can yield to Ne+Br+Br and Ne+$Br_2(B,v)$ fragmentation products, respectively. The recombination mechanism obtained from Ψ_Q will be discussed in much further detail below. Concerning the total fragmentation process from the Ψ_P portion, it should be noted that it requires that the total energy to exceed the Br_2 dissociation limit. The spectrum associated to Ψ_P, however, does not show appreciable intensity above this limit, as can be seen in Fig. 1, and therefore, the Ne +Br+Br fragmentation probability from Ψ_P shows a very low probability. Also, the spectrum associated with Ψ_Q is essentially above the $Br_2(B)$ dissociation limit, because the Ne–Br_2 interaction is very weak. As a consequence, the spectra associated with these two portions of the wave packet correspond to essentially different energy intervals, so that their overlap is very small.

As it will be described below, above the dissociation limit denser grid in r must be included as compared to that used below (in the present case by a factor of 2) to account for the large momenta involved. Also, related to this last point, the time step required is of 0.2 fs above the dissociation limit, which is 10 times shorter than that used below for Ψ_P. Therefore, in the present case, the procedure followed allows a reduction of the computational time by a factor between 10 and 20, as compared to a full calculation without approximation. This reduction affects the calculation carried out below the $Br_2(B)$ dissociation limit which involves slower processes and lower kinetic energy while the computational cost of the calculation carried out above this threshold remains essentially unchanged.

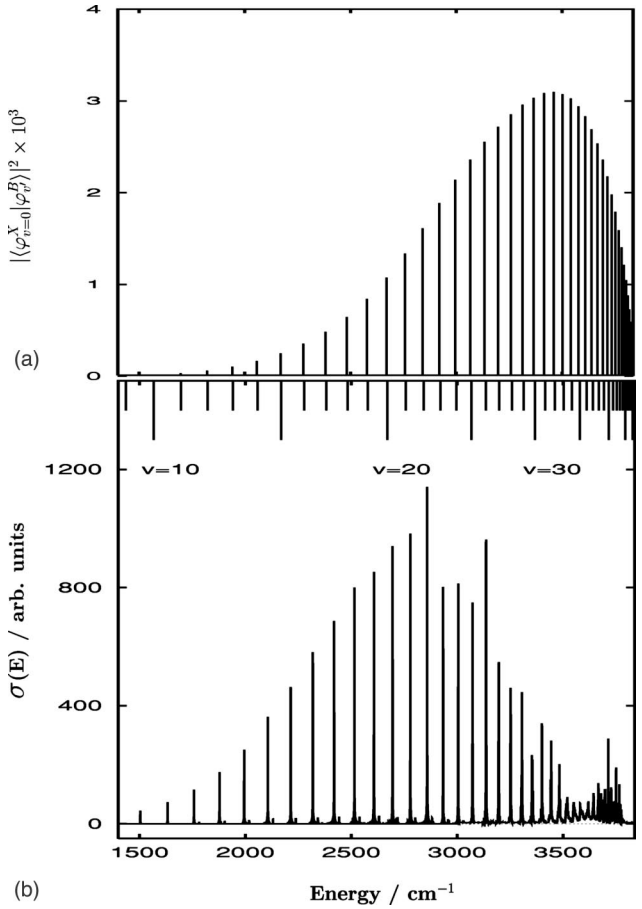

FIG. 1. (a) Square of the Franck–Condon factor for the $B\leftarrow X$ transition of isolated Br_2. (b) Absorption cross section for the $B,J=0\leftarrow X,J=1$ transitions in $NeBr_2$ complexes. Energies are referred to the minimum of the $Br_2(B)$ potential.

For the two electronic states, X and B, considered here, the interaction potential is represented as

$$V^{X,B}(r,R,\gamma)=V^{X,B}_{Br_2}(r)+W^{X,B}(r,R,\gamma). \tag{10}$$

$V^{X,B}_{Br_2}(r)$ are the intermolecular potentials of isolated Br_2 in X or B electronic states. $V^X_{Br_2}(r)$ is described by a Morse function, with parameters $D=24\,557.674$ cm^{-1}, $\alpha=1.588$ Å^{-1}, and $r_e=2.281$ Å, while $V^B_{Br_2}(r)$ is described by a RKR potential from Ref. 68. $W^{X,B}(r,R,\gamma)$ is built as a sum of pairwise Ne–Br interactions, each of them described by a Morse function of parameters $D=45$ cm^{-1}, $\alpha=1.67$ Å^{-1}, $R_e=3.7$ Å for the X state and $D=42$ cm^{-1}, $\alpha=1.67$ Å^{-1}, $R_e=3.9$ Å for the B state. This parametrization of the potential of the B state is taken from Ref. 39 and reproduces reasonably well the experimental spectral shifts and linewidths.[11,36]

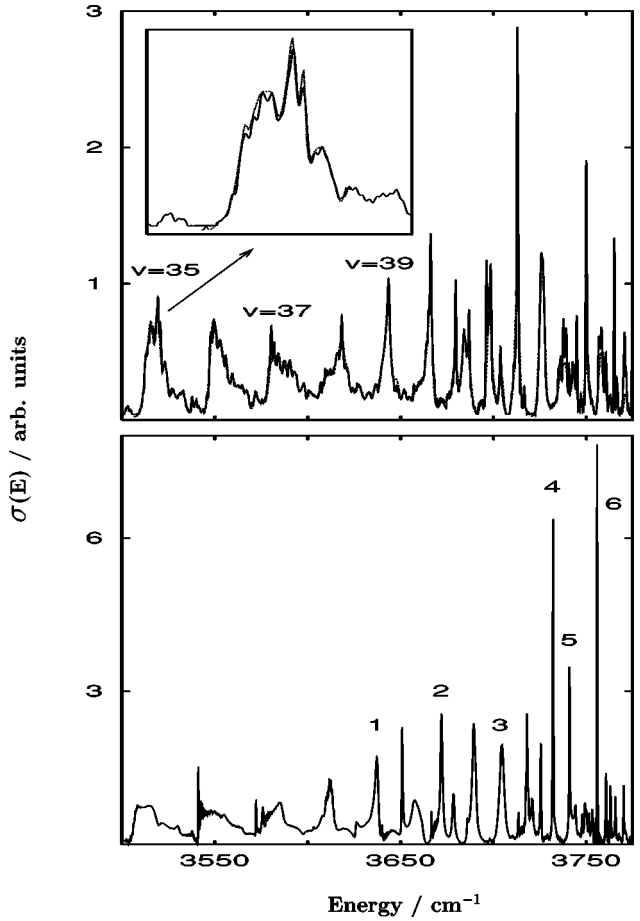

FIG. 2. Absorption cross section (solid lines) for $NeBr_2$ ($B,J'=0\leftarrow X,J=1$) transition obtained in the full dimensionality treatment (top panel) and in the two-dimensional treatment (bottom panel), obtained as the Fourier transform of autocorrelation function. In the top panel, the dashed line corresponds to the sum of the partial cross sections. Also in the top panel, the inset presents a comparison with a time-independent close-coupling treatment (in dotted lines). The numbers indicated in the bottom panel label some of the resonances presented in Fig. 5.

III. DYNAMICS BELOW THE $Br_2(B)$ DISSOCIATION LIMIT

A. Absorption spectrum

The grid used for the propagation of Ψ_P consists of 512 points for $1.8\leqslant r\leqslant 12$, 128 points for $0.1\leqslant R\leqslant 18$ (all distances in Å), and 25 Gauss–Legendre points for γ (in the $[0,\pi/2]$ interval, taking into account the Br_2 exchange symmetry). The time step used is 2 fs and the propagation has been performed until 20 ps. Since the initial wave packet is real, $\langle\Psi^{JM\epsilon}(\mathbf{R},\mathbf{r},t=0)|\Psi^{JM\epsilon}(\mathbf{R},\mathbf{r},2t)\rangle = \langle[\Psi^{JM\epsilon}(\mathbf{R},\mathbf{r},t)]^*|\Psi^{JM\epsilon}(\mathbf{R},\mathbf{r},t)\rangle$ which allows the determination of the autocorrelation function up to 40 ps. In Fig. 1, the resulting absorption cross section, obtained using Eq. (5), is compared to the square of the Franck–Condon factors of the isolated Br_2 molecule. It should be noted that in the low energy regime (<3000 cm^{-1}) the spectrum is not well converged because the resonances involved are very narrow. In this regime it is more efficient to use the close-coupling method as already done[40] on this system. For energies higher than 3000 wave numbers, however, the spectrum is rather well converged. In the top panel of Fig. 2, the absorption spectrum obtained from the autocorrelation function, Eq. (5), is compared to the result of summing the partial cross sections over all possible final states of Br_2 fragments. The agreement is excellent and is only slightly worse in the vicinity of very narrow resonances, demonstrating that the spectrum is essentially converged. We have also performed time-independent close coupling calculations[69] that compare very well with the time-dependent results, as can be seen in the inset of Fig. 2. Also, in the bottom panel of Fig. 2, we show the result of a two-dimensional calculation (2D), in which the geometry has been restricted to a T-shaped configuration. As can be seen, there is an excellent qualitative agreement between the full dimensionality (3D) and the 2D spectra as will be discussed in the next section.

Below 3000 cm^{-1} the spectrum in Fig. 1(b) shows a clear vibrational progression with well isolated resonances. These resonances essentially correspond to ground van der Waals states placed about 62 cm^{-1} below the associated $Br_2(v')$ level. Also, there are weak transitions corresponding to van der Waals excited states, shifted about 24 cm^{-1} with respect to the ground van der Waals level. The latter are approximately one order of magnitude lower in intensity than the fundamental one. A bound state calculation using the vibrational diabatic approximation[70] shows that this level corresponds to the second van der Waals excited state, $n=2$ (for the even parity block under Br_2 exchange), with a mixture of bending and stretching excitations. The first excited van der Waals state, with a binding energy of ≈ 44 cm^{-1}, corresponds to a pure excitation of the stretching mode and does not present appreciable oscillator strength.

Below $v'=27$, at ≈ 3200 cm^{-1}, fragmentation mainly occurs by the transfer of one vibrational quantum of the Br_2 subunit. In this $\Delta v=-1$ regime, it can be assumed that a single zero-order bound state, usually called ''bright'' state, corresponding to a particular v' manifold and to the ground van der Waals state, is the only one responsible of the oscillator strength in a given energy range. This ''bright'' quasibound state couples to the dissociative continua and the corresponding spectrum is well reproduced by a Lorentzian function (isolated resonance regime). In this region of the spectrum, several properties behave monotonically with the initial vibrational excitation, v', of the complex. As an example, in Fig. 3, calculated spectral shifts (for $14<v'<41$) are presented and compared with available experimental data.[11] It can be seen that it increases smoothly up to $v'=30$. In the same range, calculated shifts compare fairly well with the measured ones, indicating that the interaction potentials used in this work are rather realistic.

Above the closing of the $\Delta v=-1$ channel ($E>3200$ cm^{-1}), the spectral shift presents oscillations as a function of v', as can be seen in Fig. 3. In fact, this magnitude is not accurately defined because the spectrum corresponding to a particular $v'\leftarrow v=0$ transition splits in several peaks, as can be observed in the top panel of Fig. 2 (here, the estimated spectral shift is obtained from the position of the highest peak). Such a behavior is a manifestation of IVR in which the so called ''bright'' state couples with some other zero-order bound states of the $v'-1$ manifold. These states do not present appreciable oscillator strength and can be called

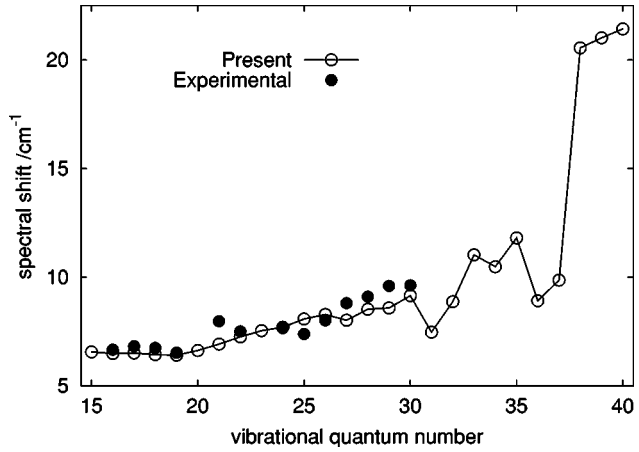

FIG. 3. Comparison between theoretical and experimental spectral shifts, as functions of the vibrational quantum number, v', of the Br_2 subunit. The experimental data are taken from Ref. 11. See text for a discussion about the assignment to the vibrational quantum numbers.

''dark'' states. Due to this IVR, the resulting spectrum loses the Lorentzian shape and exhibits several peaks.[14–16] The number of zero-order states participating in the IVR rapidly increases with energy. At about 3500 cm^{-1} the spectrum is formed by broad structures and in between them the background never goes to zero, indicating that the dynamics is reaching the intermediate-statistical IVR regime. However, these bands can still be assigned to the transitions to particular bright states (as indicated in the top panel of Fig. 2).

That the oscillator strength can be essentially attributed to a single v' channel at energies below 3500 cm^{-1} is demonstrated in Fig. 4, in which the global spectrum is compared with that obtained using a single $(v',n=0)$ ''bright'' state as initial wave packet, procedure that has been described elsewhere.[16] As can be seen in Figs. 4(a) and 4(b), this approximation works fairly well for $v'=30$ and 35, respectively. However, the approximation completely fails above $\approx$3650 cm^{-1}, as can be seen for the $v'=40$ and 45 cases in Figs. 4(c) and 4(d), respectively. Since the global spectrum is very well converged in this energy range, we attribute all differences to the lack of adequacy of the ''bright'' state approximation. Hence, it is not appropriate to assign the transitions to any particular v' vibrational level for the higher energy range of the spectrum. The number of vibrational quanta needed to dissociate the complex is therefore a magnitude that has no significant meaning at this level.

The failure of the ''bright'' state approximation is one, but not the unique, indication of a change in the qualitative behavior of the $NeBr_2$ spectroscopy and dynamics above $\approx$3650 cm^{-1}. Just before this energy, the maxima of the bands ($v'=38,39$) shift markedly to higher energies, as can be clearly seen in Fig. 3. Also, one would expect that the density of states will continue to increase. It is notorious that the spectrum above 3600 cm^{-1} (in Figs. 1 and 2) becomes quite structured, as in the intermediate-sparse IVR limit, and relatively narrow resonances can be clearly distinguished. Such narrow resonances cannot be described within the ''bright'' approximation probably because the separation of the two bromine atoms increases significantly near the dissociation threshold and all modes are strongly mixed. The appearance of so long-lived resonances at such high energies is rather surprising and indeed deserves further analysis.

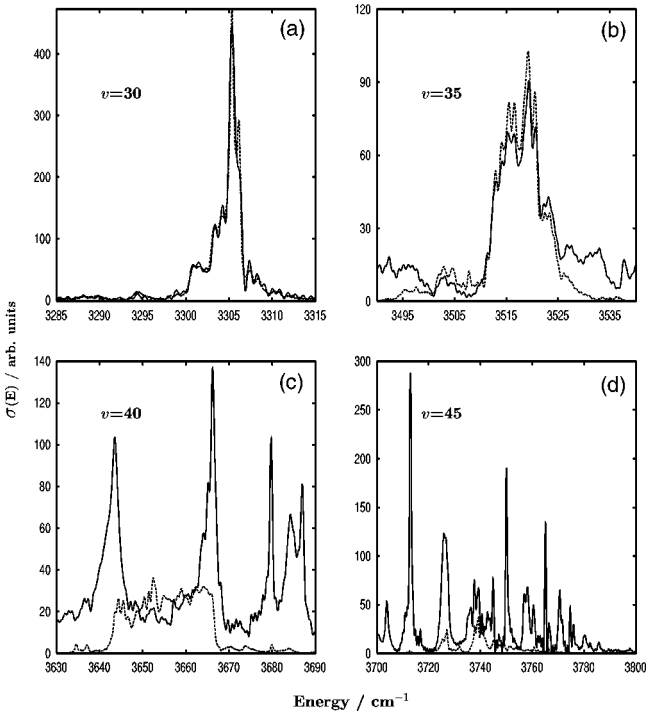

FIG. 4. Absorption spectrum obtained using an ''exact'' treatment (solid lines), as described in this work, and using the ''bright state'' approximation (dashed lines), discussed in the text, for different $NeBr_2(B,J'=0,v'\leftarrow X,J=1,v=0)$ transitions: (a) $v'=30$; (b) $v'=35$; (c) $v'=40$; and (d) $v'=45$.

B. Resonances near the Br_2 dissociation limit

A simplified two-dimensional (2D) model calculation is carried out, in which the angle γ is fixed to $\pi/2$. Such a model allows us to perform more accurate calculations (by using denser grids and longer propagation times) and, in addition, simpler interpretations of the underlying processes can be found. A grid of 2048 points for $1.8\leqslant r\leqslant 27$ Å and 256 for $0.25\leqslant R\leqslant 30$ Å was used and the equations were integrated up to 55 ps with a time interval of 2 fs. The spectrum thus obtained is shown in the bottom panel of Fig. 2. This spectrum is remarkably similar to that obtained in the three-dimensional case, including all major features. Narrow resonances appear at nearly the same energy (above 3600 cm^{-1}) and exhibit a similar spacing to that of the three-dimensional calculations, and suggests that they have the same origin.

In order to analyze those resonances, a pseudo spectral method is used,[52,71,72] in which an approximated quasibound state, ϕ_n^0, is obtained as

$$\phi_n^0 \approx \mathrm{Re}\int_0^\infty dt e^{i(E_n+i\Gamma_n)t/\hbar}\Psi(R,r,t), \tag{11}$$

where E_n and Γ_n are the approximate position and width of the resonances, respectively. The amplitude density contour plots associated with some of the resonances (marked by a

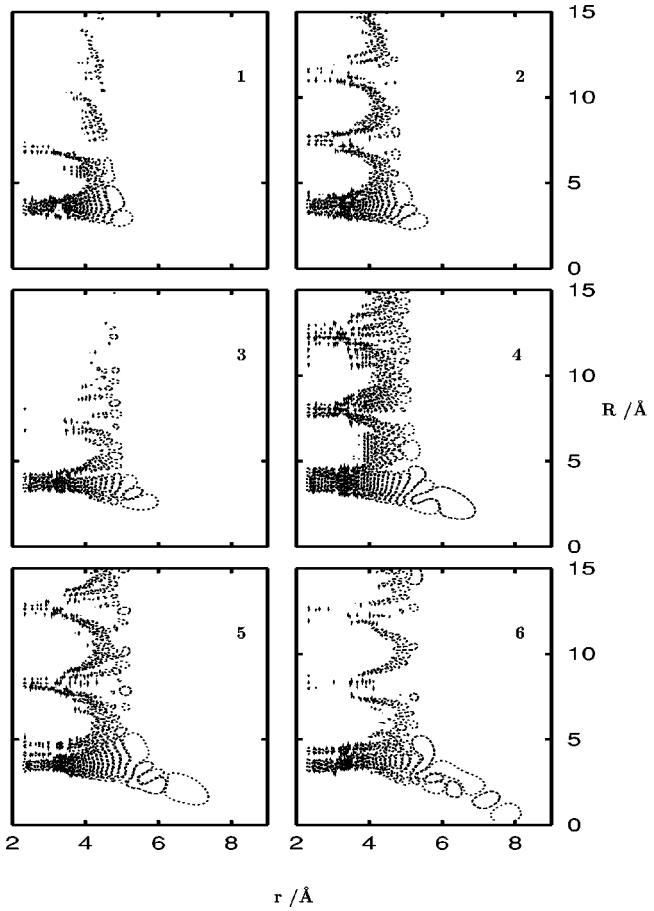

FIG. 5. Contour plots of the amplitude density associated with some of the resonances (marked with a number) appearing in the spectrum of the lower panel of Fig. 2.

number in Fig. 2) are shown in Fig. 5. As energy increases, the two Br atoms separate and the Ne atom inserts between them. For $R \leqslant 4$ Å the regular nodal structure associated with the resonances resembles that of ''horseshoe'' states,[73] in which the Ne atom approaches (moves away) the Br_2 center-of-mass while simultaneously the Br_2 bond is lengthened (shortened).

For larger R, there is a sequence of such ''horseshoe'' structures as Ne goes away leaving the Br_2 fragment vibrating. The departure of the Ne atom starts at short values of r, where the vibrational energy transfer is more likely to occur. As energy increases, the maximum of the amplitude density of the resonances shifts towards smaller R and larger r values. At these configurations, vibrational energy transfer to continuum dissociative states is very inefficient, which explains the long lifetimes of the resonances appearing at so high energies. These ''horseshoe'' states might also hardly couple with the rather dense manifold of intermediate ''dark'' states, in contrast with the situation of the intermediate-statistical regime of IVR in the lower energy region of the spectrum. Because the ''horseshoe''-like states may be considered as bright states in this spectral region and are inefficiently coupled to intermediate ''dark'' states as well as to dissociative state, the effective density of states in the spectrum decreases towards a more structured sparse limit near the $Br_2(B)$ dissociation limit. Experimental detection of these resonances would provide interesting information on the potential energy surface at very long Br_2 internuclear distances.

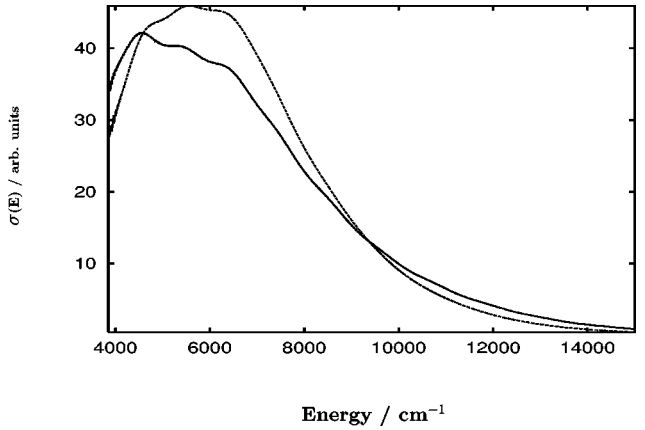

FIG. 6. Absorption cross section above the $Br_2(B)$ dissociation threshold (located at ≈ 3840 cm^{-1}), for the $NeBr_2$ complex (solid line) and for bare Br_2 molecule (dashed line).

IV. DYNAMICS ABOVE THE $Br_2(B)$ DISSOCIATION LIMIT

A. Total spectrum and recombination probabilities

The absorption spectrum above the $Br_2(B)$ dissociation threshold, in Fig. 6, is spread out in energy. For this reason, the number of radial points in the grid of r has been augmented to 1024, in the same interval as that used below the threshold, in order to properly account for such high kinetic energies. Since r is the variable directly reached through optical excitation, this is the coordinate in which most of the energy is deposited and, hence, the other two internal degrees of freedom are reasonably well described using the same grids as those used below the threshold. The time step used is of 0.2 fs and the propagation was performed until 2.7 ps, time at which $\approx 98\%$ of the wave packet is absorbed.

The spectrum in Fig. 6 presents a shift towards lower energies than that of bare Br_2. Small oscillations at low energies are present in the two cases, and are due to features of the dissociative wave functions of bare $Br_2(B)$, which originate maxima in the overlap between the $Br_2(X, v=0)$ and the dissociative wave functions.

In the present three-dimensional quantum mechanical calculations the recombination cross section obtained, in Fig. 7, is very small as compared to the total cross section (by about 4 order of magnitudes!). Although it is very small, the recombination probability presents several features that cannot be simply attributed to numerical errors. First, it decreases monotonically with energy, nothing related to a ''white noise.'' Second, the recombination flux appears at relatively long propagation times, suggesting that, as could be expected, Br_2 products are formed in high vibrational states and hence with associated low kinetic energies.

The final rotational distributions of the recombined Br_2 fragments, in Fig. 8, exhibit maxima at a low j followed by a nearly monotonous decrease as j increases, for all the energies considered. These distributions are very similar to the

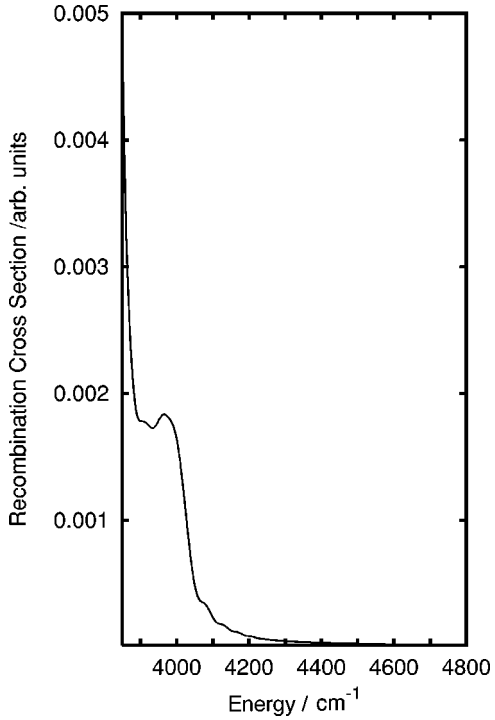

FIG. 7. Total recombination cross section when exciting the $NeBr_2$ complex above the Br_2 dissociation threshold after 2.7 ps of propagation of the full dimensional wave packet. Note the small cross sections, about four orders of magnitudes smaller than the total absorption cross section shown in Fig. 6.

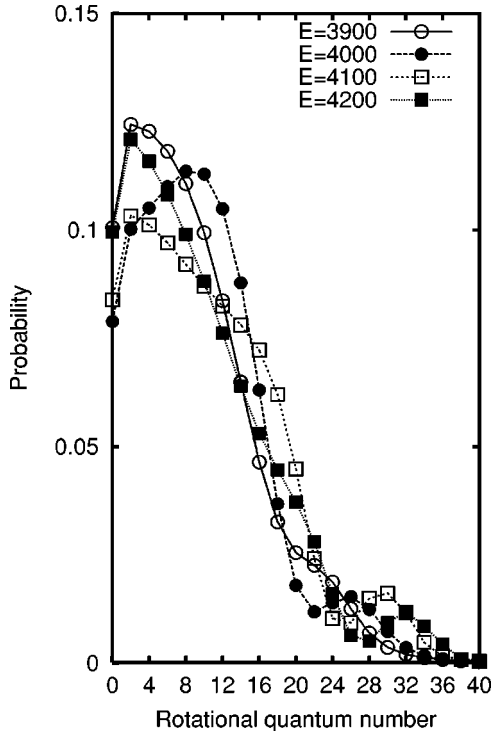

FIG. 8. Final rotational distribution of the Br_2 fragments obtained by recombination when exciting the $NeBr_2$ complex above the Br_2 dissociation threshold at different total energies.

decomposition of the initial state, $\Psi_i^{J_i M_i \epsilon_i}$, into free rotor functions. This means that the complex does not change significantly its angular configuration (predominantly T-shaped) during dissociation. This fact could explain why the recombination probability is so small: during dissociation, the Ne atom does not approach a collinear configuration (Br–Br–Ne), where recombination is expected to be more important.

The assumption of the collinear as the preferred geometry for recombination is based on kinematic models, like that of Valentini and Cross.[46] In that model, formulated for the above-threshold recombination in the related ArI_2 system, I_2 is recombined after a single, impulsive collision between Ar and the middle I when I_2 is dissociating within I–I–Ar (one-atom cage effect). Quasiclassical trajectories (QCT) calculations on the same system confirmed that collinear are more efficient than perpendicular configurations for recombination.[42,43]

B. Two-dimensional calculation of recombination probabilities

The fact that the dissociation above the $Br_2(B)$ threshold proceeds at a nearly T-shaped geometry, allows us to check the recombination probabilities within the corresponding two-dimensional model, for which more extensive convergence tests can be done as well as longer propagation times can be reached. Thus, we have performed calculations in the above mentioned large bidimensional grid and the propagation has been performed up to 10 ps. The recombination probability at 2.7 ps (time at which the full dimensional calculations ended) is shown in Fig. 9 and is in good agreement with the corresponding full dimensional results, in Fig. 7. However, as time proceeds the recombination probability increases significantly, becoming of the order of one tenth of the total absorption probability at about zero kinetic energy and 10 ps. Such a delay in the arrival of the recombined Br_2 products to the absorbing edge, where they are analyzed, is of course a result of the low kinetic energy available.

The vibrational distribution of the recombined $Br_2(B,v'')$ products, in Fig. 10, starts being appreciable at $v''=29$. Since $Br_2(B)$ supports 52 vibrational levels, about 20 vibrational quanta (400–500 cm^{-1}) are transferred at nearly zero kinetic energy. A significant energy transfer was observed by Philippoz and co-workers[44] in the case of ArI_2; they found that the final I_2 vibrational distributions are peaked between $v''=40$ and 50, depending on the excitation wavelength. Although they did not measure the total recombination probability, they were able to obtain the I_2 vibrational distribution even though it occurred with a very small probability, since the fluorescence of $I_2(B,v'')$ is easily recorded and it corresponds to a wavelength very different from the excitation one.

However, it is probably not appropriate to establish a direct parallelism between Philippoz *et al.* observations on ArI_2 and our results on $NeBr_2$, since it is very likely that I_2 recombination occurs starting from a linear isomer (I–I–Ar) in the *X* electronic state and not from a T-shaped one as is the present case of $NeBr_2$. Klemperer and co-workers[33,48] proposed the existence of a linear isomer for $ArI_2(X)$ to explain some observations in the $ArI_2(B)$ photodissociation. The existence of linear isomers has been confirmed by highly accurate *ab initio* calculations[74] and has also been found in other

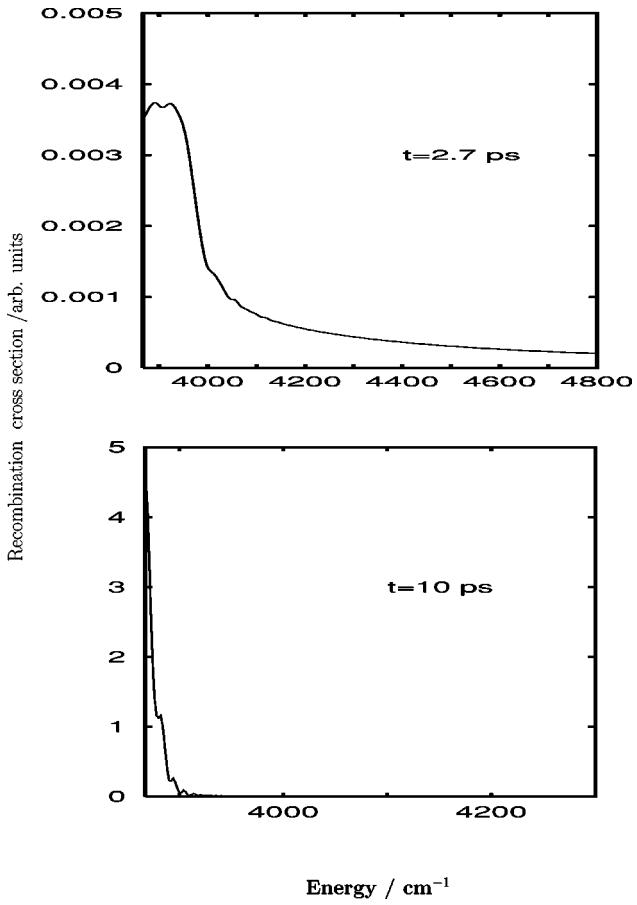

FIG. 9. Total recombination cross section for the bidimensional model at T-shaped geometry, at 2.7 ps (top panel) and at 10 ps (bottom panel).

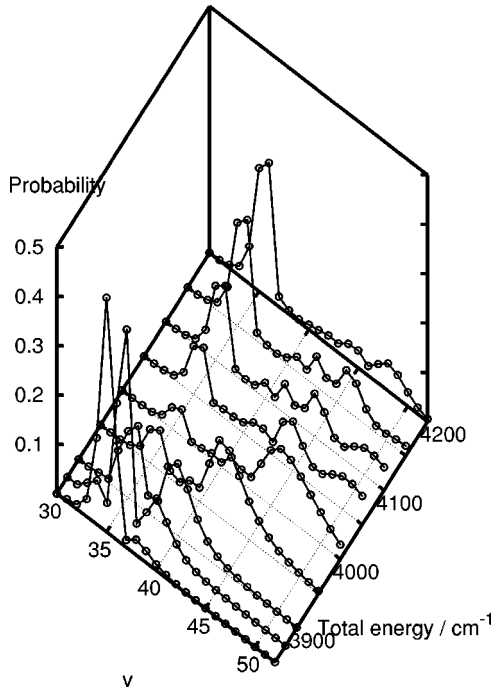

FIG. 10. Final vibrational distribution of the recombined Br_2 fragments when exciting the $NeBr_2$ complex at different total energies above the Br_2 dissociation threshold, obtained within the two-dimensional model.

complexes of Cl_2.[33,49,75–79] Moreover, the Philippoz *et al.* vibrational distributions have been successfully reproduced by recent calculations[50,51] where the dominant geometry during the dynamical process is the collinear one.

In this regard, it would be worthwhile to investigate the existence of a linear isomer in the $NeBr_2(X)$ potential energy surface, by means of accurate *ab initio* calculations, and then to study the dynamics of the above-threshold recombination from the collinear configuration. Analogies and differences with the ArI_2 dynamics could be then established in a more complete manner. Another process to compare with would be the photodissociation of linear Ar–HCl (Refs. 80–82) or Ar–HBr.[83] In these cases, the hydrogen halide is excited to a repulsive state and the recombination is not possible unless nonadiabatic processes would involve a change to a bound electronic state. The cage effect manifests itself in the final kinetic energy distribution of the H fragment.[84] Very recently, ArCl diatomic fragments have been obtained[82] as a result of the fast scaping H atoms and the attractive Ar–Cl interaction. It would be interesting to investigate if such an effect is also possible from a linear (Br–Br–Ne) isomer.

V. CONCLUSIONS

In this work, extensive three-dimensional wave packet calculations of the photodissociation dynamics of $NeBr_2$ are presented corresponding to a $B \leftarrow X$ transition. The calculations were split into two separated runs, one corresponding to the bound region of the $Br_2(B)$ state and the second to its continuum part. This procedure is a good approximation, because the two spectra do not noticeably overlap, and it allows us to reduce significantly the computational cost. This method can be generalized to divide the wave packet in more portions especially in energy regions where the spectrum corresponds to well isolated lines.

In the bound region of $Br_2(B)$, special attention has been paid to the high vibrational excitation region where the spectrum becomes rather congested. Thus, the absorption, corresponding to a single v' level at low vibrational excitations, is no longer possible to be assigned to a particular set of v's. As energy increases, the spectrum does not show a progressive congestion, as a consequence of the natural increment of the density of states. On the contrary, near the threshold, it seems that the spectrum becomes very structured again and formed by relatively long-lived resonances. Such alternative behavior between congested-sparse regimes might be associated with regular trajectories.

The long lived resonances near the $Br_2(B)$ dissociation limit has been analyzed considering a two-dimensional model. The absorption spectrum in this case is extraordinarily similar to that obtained in the three-dimensional calculations that confirms the robustness of the interpretation. Thus, the resonances correspond to ''horseshoe'' states in which the Ne atom is vibrating in and out the middle of the Br_2 molecule. The vibrational energy transfer mainly takes place when the Br_2 internuclear distance becomes small. The probability density associated with these ''horseshoe'' type resonances shifts towards large r values. The coupling of these states with the dissociative states becomes very inefficient so that resonance lifetimes are very long. The inefficiency of the

coupling could also be the explanation for the ''sparseness'' of the spectrum at these energies, because the ''horseshoe'' states should not couple either to the dense manifold of intermediate ''dark'' states. Experimental examination of those resonances could provide valuable information of the potential energy surface at rather large interhalogen distances. These resonances are probably only accessible from T-shaped minima in the $NeBr_2(X)$ and not from a linear isomer, if it exists.

Above the $Br_2(B)$ dissociation continuum, the spectrum is rather similar to that of bare Br_2 and is spread over a large energy region of ≈ 2 eV. The formation of $Br_2(B,v'')$ as a consequence of a recombination process induced by the presence of the Ne atom is analyzed. Three-dimensional calculations have been performed until 2.7 ps. At this time the recombination cross section is about four orders of magnitude smaller than the total absorption cross section at low total energies, and decreases very fast with total energy. The rotational distribution of recombined Br_2 fragments is consistent with a nearly T-shaped geometry during the dissociation process. Thus, extensive bidimensional calculations have been performed until longer times, 10 ps. It is found that the recombination cross section increases significantly, becoming about one-tenth of the total absorption cross section.

The recombination probability should be much larger when exciting the complex from a linear isomer, if it exists, following a impulsive mechanism.[46] Since several related systems present a linear isomer in the X state,[78] it seems interesting to analyze the existence of a linear well on the X state of the complex. For that purpose, highly accurate *ab initio* calculations are being currently performed on the ground electronic state of the $NeBr_2$ complex.

ACKNOWLEDGMENTS

We thank Professor K. C. Janda for very fruitful discussions and for calling our attention to this system. This work has been supported by DGICYT (Ministerio de Educación y Ciencia, Spain) under Grant No. PB95-0071, and by the European TMR network Contract No. HPRN-CT-1999-0005.

[1] *Structure and Dynamics of Weakly Bound Molecular Complexes*, edited by A. Weber (Reidel, Dordrecht, 1987).
[2] *Dynamics of Polyatomic van der Waals Complexes*, edited by N. Halberstadt and K. C. Janda (Plenum, New York, 1990).
[3] A. Rohrbacher, N. Halberstadt, and K. C. Janda, Annu. Rev. Phys. Chem. **51**, 405 (2000).
[4] J. A. Beswick and J. Jortner, Adv. Chem. Phys. **47**, 363 (1981).
[5] G. E. Ewing, J. Chem. Phys. **71**, 3143 (1979).
[6] K. E. Johnson, L. Wharton, and D. H. Levy, J. Chem. Phys. **69**, 2719 (1978).
[7] M. Gutmann, D. M. Willberg, and A. H. Zewail, J. Chem. Phys. **97**, 8037 (1992).
[8] J. I. Cline, B. P. Reid, D. D. Evard, N. Sivakumar, N. Halberstadt, and K. C. Janda, J. Chem. Phys. **89**, 3535 (1988).
[9] J. E. Kenny, K. E. Johnson, W. Sharfin, and D. H. Levy, J. Chem. Phys. **72**, 1109 (1980).
[10] D. M. Willberg, M. Gutmann, J. J. Breen, and A. H. Zewail, J. Chem. Phys. **96**, 198 (1991).
[11] B. A. Swartz, D. E. Brinza, C. M. Western, and K. C. Janda, J. Phys. Chem. **88**, 6272 (1984).
[12] J. I. Cline, N. Sivakumar, D. D. Evard, C. R. Bieler, B. P. Reid, N. Halberstadt, S. R. Hair, and K. C. Janda, J. Chem. Phys. **90**, 2605 (1989).
[13] D. D. Evard, C. R. Bieler, J. I. Cline, N. Sivakumar, and K. C. Janda, J. Chem. Phys. **89**, 2829 (1988).
[14] N. Halberstadt, S. Serna, O. Roncero, and K. C. Janda, J. Chem. Phys. **97**, 341 (1992).
[15] O. Roncero, P. Villarreal, G. Delgado-Barrio, N. Halberstadt, and K. C. Janda, J. Chem. Phys. **99**, 1035 (1993).
[16] O. Roncero, D. Caloto, K. C. Janda, and N. Halberstadt, J. Chem. Phys. **107**, 1406 (1997).
[17] S. K. Gray, Chem. Phys. Lett. **197**, 86 (1992).
[18] S. K. Gray and O. Roncero, J. Phys. Chem. **99**, 2512 (1995).
[19] O. Roncero and S. K. Gray, J. Chem. Phys. **104**, 4999 (1996).
[20] L. J. van der Burgt, J. P. Nicolai, and M. C. Heaven, J. Chem. Phys. **81**, 5514 (1984).
[21] D. G. Jahn, S. G. Clement, and K. C. Janda, J. Chem. Phys. **101**, 283 (1994).
[22] T. González-Lezana, M. I. Hernández, G. Delgado-Barrio, A. A. Buchachenko, and P. Villarreal, J. Chem. Phys. **105**, 7454 (1996).
[23] T. González-Lezana, M. I. Hernández, G. Delgado-Barrio, and P. Villarreal, J. Chem. Phys. **106**, 3216 (1997).
[24] A. Rohrbacher, Th. Ruchti, K. C. Janda, A. A. Buchachenko, M. I. Hernández, T. González-Lezana, P. Villarreal, and G. Delgado-Barrio, J. Chem. Phys. **110**, 256 (1999).
[25] G. Kubiak, P. S. H. Fitch, L. Wharton, and D. H. Levy, J. Chem. Phys. **68**, 4477 (1978).
[26] J. A. Blazy, B. M. DeKoven, T. D. Russell, and D. H. Levy, J. Chem. Phys. **72**, 2439 (1980).
[27] K. E. Johnson, W. Sharfin, and D. H. Levy, J. Chem. Phys. **74**, 163 (1981).
[28] D. H. Levy, Adv. Chem. Phys. **47**, 323 (1981).
[29] J. J. Breen, D. M. Willberg, M. Gutmann, and A. H. Zewail, J. Chem. Phys. **93**, 9180 (1990).
[30] M. L. Burke and W. Klemperer, J. Chem. Phys. **98**, 6642 (1993).
[31] O. Roncero, N. Halberstadt, and J. A. Beswick, J. Chem. Phys. **104**, 7554 (1996).
[32] E. M. Goldfield and S. K. Gray, Chem. Phys. Lett. **276**, 1 (1997).
[33] A. E. Stevens Miller, Ch. Chuang, H. C. Fu, K. F. Higgins, and W. Klemperer, J. Chem. Phys. **111**, 7844 (1999).
[34] A. A. Buchachenko and N. F. Stepanov, J. Chem. Phys. **104**, 9913 (1996).
[35] F. Y. Naumkin, Chem. Phys. **226**, 319 (1998).
[36] J. I. Cline, D. D. Evard, B. P. Reid, N. Sivakumar, F. Thommen, and K. C. Janda, *Structure and Dynamics of Weakly Bound Molecular Complexes*, edited by A. Weber (Reidel, Dordrecht, 1987), p. 533.
[37] N. Sivakumar, J. I. Cline, C. R. Bieler, and K. C. Janda, Chem. Phys. Lett. **147**, 561 (1988).
[38] M. Nejad-Sattari and T. A. Stephenson, J. Chem. Phys. **106**, 5454 (1997).
[39] A. A. Buchachenko, A. Y. Baisogolov, and N. F. Stepanov, J. Chem. Soc., Faraday Trans. **90**, 3229 (1994).
[40] T. A. Stephenson and N. Halberstadt, J. Chem. Phys. **112**, 2265 (2000).
[41] B. Miguel, A. Bastida, J. Zúñiga, A. Requena, and N. Halberstadt, J. Chem. Phys. **113**, 10130 (2000).
[42] I. NoorBatcha, L. M. Raff, and D. L. Thompson, J. Chem. Phys. **81**, 5658 (1984).
[43] M. Miranda, J. A. Beswick, and N. Halberstadt, Chem. Phys. **187**, 185 (1994).
[44] J. M. Philippoz, P. Melinon, R. Monot, and H. van den Bergh, Chem. Phys. Lett. **91**, 2545 (1987).
[45] K. L. Saenger, G. M. McClelland, and D. R. Herschbach, J. Phys. Chem. **85**, 3333 (1981).
[46] J. J. Valentini and J. B. Cross, J. Chem. Phys. **77**, 572 (1982).
[47] J. M. Philippoz, R. Monot, and H. van den Bergh, J. Chem. Phys. **93**, 8676 (1990).
[48] M. L. Burke and W. Klemperer, J. Chem. Phys. **98**, 1797 (1993).
[49] A. Burroughs, T. Van Marter, and M. C. Heaven, J. Chem. Phys. **111**, 2478 (1999).
[50] J.-Y. Fang and C. C. Martens, J. Chem. Phys. **105**, 9072 (1996).
[51] S. Zamith, C. Meier, N. Halberstadt, and J. A. Beswick, J. Chem. Phys. **110**, 960 (1999).
[52] M. Paniagua, A. Aguado, M. Lara, and O. Roncero, J. Chem. Phys. **111**, 6712 (1999).
[53] R. N. Zare, *Angular Momentum* (Wiley, New York, 1988).
[54] A. Aguado, M. Paniagua, M. Lara, and O. Roncero, J. Chem. Phys. **107**, 10085 (1997).
[55] H. Tal-Ezer and R. Kosloff, J. Chem. Phys. **81**, 3967 (1984).
[56] R. Kosloff, J. Phys. Chem. **92**, 2087 (1988).
[57] D. Neuhauser and M. Baer, J. Chem. Phys. **91**, 4651 (1989).

[58] R. S. Judson, D. J. Kouri, D. Neuhauser, and M. Baer, Phys. Rev. A **42**, 351 (1990).
[59] D. Neuhauser and M. Baer, J. Chem. Phys. **92**, 3419 (1990).
[60] J. C. Light, I. P. Hamilton, and J. V. Lill, J. Chem. Phys. **82**, 1400 (1985).
[61] A. C. Peet and W. Yang, J. Chem. Phys. **91**, 6598 (1989).
[62] J. T. Muckerman, Chem. Phys. Lett. **173**, 200 (1990).
[63] G. C. Corey, J. W. Tromp, and D. Lemoine, in *Numerical Grid Methods and Their Application to the Schrödinger Equation*, edited by C. Cerjan (Kluwer Academic, New York, 1993).
[64] O. A. Sharafeddin and J. C. Light, J. Chem. Phys. **102**, 3622 (1995).
[65] E. J. Heller, J. Chem. Phys. **68**, 2066 (1978).
[66] E. J. Heller, J. Chem. Phys. **68**, 3891 (1978).
[67] G. G. Balint-Kurti, R. N. Dixon, and C. C. Marston, J. Chem. Soc., Faraday Trans. **86**, 1741 (1990).
[68] R. F. Barrow, T. C. Clark, J. A. Coxon, and K. K. Lee, J. Mol. Spectrosc. **51**, 428 (1974).
[69] O. Roncero, J. A. Beswick, N, Halberstadt, P. Villarreal, and G. Delgado-Barrio, J. Chem. Phys. **92**, 3348 (1990).
[70] J. A. Beswick and G. Delgado-Barrio, J. Chem. Phys. **73**, 3653 (1980).
[71] R. Sadeghi and R. T. Skodje, J. Chem. Phys. **102**, 193 (1995).
[72] C. L. Russell and D. E. Manolopoulos, Chem. Phys. Lett. **256**, 465 (1996).
[73] J. Tennyson, O. Brass, and E. Pollak, J. Chem. Phys. **92**, 3005 (1990).
[74] Ch. F. Kunz, I. Burghardt, and B. A. He$\beta\beta$, J. Chem. Phys. **109**, 359 (1998).
[75] S. S. Huang, C. R. Bieler, K. C. Janda, F. Tao, W. Klemperer, P. Casavecchia, G. G. Volpi, and N. Halberstadt, J. Chem. Phys. **102**, 8846 (1995).
[76] J. Williams, A. Rohrbacher, J. Seong, N. Marianayagam, K. C. Janda, R. Burcl, M. M. Szczesniak, G. Chalasinski, S. M. Cybulski, and N. Halberstadt, J. Chem. Phys. **111**, 997 (1999).
[77] S. M. Cybulski and J. S. Holt, J. Chem. Phys. **110**, 7745 (1999).
[78] A. Rohrbacher, J. Williams, and K. C. Janda, Phys. Chem. Chem. Phys. **1**, 5263 (1999).
[79] A. A. Buchachenko, O. Roncero, and N. F. Stepanov, Russ. J. Phys. Chem. **74**, S193 (2000).
[80] A. García-Vela, J. Chem. Phys. **108**, 5755 (1998).
[81] J. C. Juanes-Marcos and A. García-Vela, J. Chem. Phys. **111**, 2606 (1999).
[82] J. C. Juanes-Marcos and A. García-Vela, J. Chem. Phys. **112**, 4983 (2000).
[83] M. Monnerville and B. Pouilly, Chem. Phys. Lett. **294**, 473 (1998).
[84] A. García-Vela, R. B. Gerber, and J. J. Valentini, J. Chem. Phys. **97**, 3297 (1992).